MICRON-SIZED PARTICLE IMPACTS DETECTED NEAR URANUS BY THE VOYAGER 2 PLASMA WAVE INSTRUMENT

by

D. A. Gurnett[1], W. S. Kurth[1], F. L. Scarf[2], J. A. Burns[3], J. N. Cuzzi[4] and E. Grün[5]

Department of Physics and Astronomy
THE UNIVERSITY OF IOWA
Iowa City, Iowa 52242

U. of Iowa 86-40

MICRON-SIZED PARTICLE IMPACTS DETECTED NEAR URANUS BY THE VOYAGER 2 PLASMA WAVE INSTRUMENT

by

D. A. Gurnett[1], W. S. Kurth[1], F. L. Scarf[2],
J. A. Burns[3], J. N. Cuzzi[4] and E. Grün[5]

December 1986

[1]Department of Physics and Astronomy, University of Iowa, Iowa City, Iowa 52242

[2]TRW Space and Technology Group, One Space Park, Redondo Beach, California 90278

[3]Center for Radiophysics and Space Research, Cornell University, Ithaca, New York 14853

[4]Ames Research Center, Moffett Field, California 94035

[5]Max-Planck-Institut für Kernphysik, Postfach 103980, 6900 Heidelberg, West Germany

UNCLASSIFIED

SECURITY CLASSIFICATION OF THIS PAGE (When Data Entered)

REPORT DOCUMENTATION PAGE

READ INSTRUCTIONS BEFORE COMPLETING FORM

1. REPORT NUMBER: U. of Iowa 86-40

2. GOVT ACCESSION NO.:

3. RECIPIENT'S CATALOG NUMBER:

4. TITLE (and Subtitle): MICRON-SIZED PARTICLE IMPACTS DETECTED NEAR URANUS BY THE VOYAGER 2 PLASMA WAVE INSTRUMENT

5. TYPE OF REPORT & PERIOD COVERED: Progress December 1986

6. PERFORMING ORG. REPORT NUMBER:

7. AUTHOR(s): D. A. Gurnett, W. S. Kurth, F. L. Scarf, J. A. Burns, J. N. Cuzzi and E. Grun

8. CONTRACT OR GRANT NUMBER(s): N00014-85-K-0404

9. PERFORMING ORGANIZATION NAME AND ADDRESS:
Dept. of Physics and Astronomy
The University of Iowa
Iowa City, IA 52242

10. PROGRAM ELEMENT, PROJECT, TASK AREA & WORK UNIT NUMBERS:

11. CONTROLLING OFFICE NAME AND ADDRESS:
Office of Naval Research
Electronics Program Office
Arlington, VA 22217

12. REPORT DATE: 22 December 1986

13. NUMBER OF PAGES: 51

14. MONITORING AGENCY NAME & ADDRESS(if different from Controlling Office):

15. SECURITY CLASS. (of this report): UNCLASSIFIED

15a. DECLASSIFICATION/DOWNGRADING SCHEDULE:

16. DISTRIBUTION STATEMENT (of this Report)

Approved for public release; distribution is unlimited.

17. DISTRIBUTION STATEMENT (of the abstract entered in Block 20, if different from Report)

18. SUPPLEMENTARY NOTES

Submitted for publication to J. Geophys. Res.

19. KEY WORDS (Continue on reverse side if necessary and identify by block number)

Uranus rings
spacecraft dust impacts
Voyager

20. ABSTRACT (Continue on reverse side if necessary and identify by block number)

(See following page)

DD FORM 1 JAN 73 1473 EDITION OF 1 NOV 65 IS OBSOLETE
S/N 0102-LF-014-6601

UNCLASSIFIED

SECURITY CLASSIFICATION OF THIS PAGE (When Data Entered)

ABSTRACT

During the Voyager 2 flyby of Uranus, the plasma wave and radio astronomy instruments detected a region of impulsive noise near the equatorial plane just inside the orbit of Miranda, at a radial distance of 4.51 R_U. This noise is believed to be caused by micron-sized particles hitting the spacecraft. Analysis of various coupling mechanisms shows that when a dust particle hits the spacecraft at a high velocity, the particle is instantly vaporized and ionized, thereby releasing a cloud of charged particles, some of which are collected by the antenna. The resulting voltage pulse is detected by the plasma wave instrument. Based on reasonable assumptions about the charge yield and collection efficiency of the antenna, the number density and mass of the particles can be estimated from the rate and amplitude of the voltage pulses. The analysis shows that the maximum number density of the particles is about 1.6×10^{-3} m^{-3}, and the thickness of the impact region, based on a Gaussian fit, is 3480 km. The maximum number density occurs slightly after the ring plane crossing at a distance of about 280 km from the equatorial plane. The mass threshold for detecting the particles is estimated to be about 4.5×10^{-10} gm, and the rms mass of the particles is about 2.6×10^{-9} gm. For a density of a few gm cm^{-3}, the particles have radii on the order of a few microns. Possible sources for these particles include the rings,

the small satellite 1985U1 discovered outside the ring system, or other unseen small bodies that lie between synchronous orbit (3.15 R_U) and 4.51 R_U. If the particles are charged, electromagnetic forces produced by the rotating tilted dipole of Uranus may play a role in their transport and diffusion.

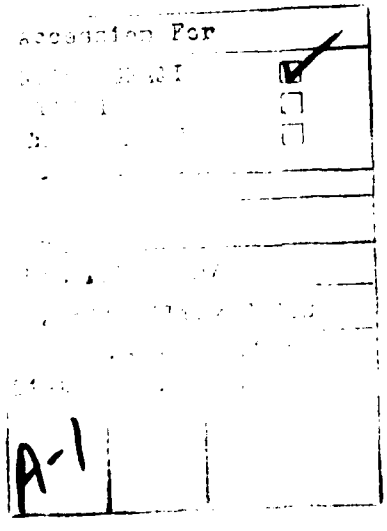

I. INTRODUCTION

During the Voyager 2 flyby of Uranus on January 24, 1986, both the plasma wave and radio astronomy instruments detected a region of impulsive noise near the equatorial plane. This noise is believed to be caused by micron-sized particles hitting the spacecraft [Gurnett et al., 1986a; Meyer-Vernet et al., 1986]. The general character of the noise is very similar to the particle impacts detected by Voyager 2 at the Saturn ring plane crossing [Scarf et al., 1982; Warwick et al., 1982; Aubier et al., 1983; Gurnett et al., 1983] and by the International Cometary Explorer during the flyby of the comet Giacobini-Zinner [Gurnett et al., 1986b; Scarf et al., 1986]. As currently understood, the noise is an electrical effect produced when a dust particle hits a spacecraft at a high velocity. At velocities above a few km/sec the particle is vaporized and produces a transient cloud of plasma that rapidly expands away from the impact site. Some of the charge released is collected by the antenna and spacecraft body, thereby causing a voltage pulse that is detected by the receiver. Laboratory measurements show that the charge released is proportional to the mass of the impacting particle. Given reasonable assumptions about the charge yield and collection efficiency of the antenna, the mass and size of the particles can be estimated. The number density can also be determined from the impact rate and knowledge of the spacecraft velocity and cross-sectional area.

In this paper we present a detailed study of the impact effects observed by the plasma wave experiment at Uranus. The objectives are (1) to give a detailed description of the impact-generated noise, (2) to analyze the mechanisms involved in coupling the impacts to the antenna, (3) to interpret the impact noise in terms of the number density and mass of the particles, and (4) to discuss the origin of the particles.

II. OBSERVATIONS

Before describing the detailed observations, it is useful to briefly review the relevant characteristics of the Voyager plasma wave instrument and the Voyager 2 trajectory by Uranus. The plasma wave experiment uses two antennas, each 10 m long and 1.3 cm in diameter, mounted in a V configuration as shown in Figure 1. The antennas are operated as an electric dipole, which means that the instrument responds to the voltage difference between the two antenna elements. The instrument processes signals from the antennas in two ways. First, a broadband receiver is used to provide waveforms of the received signals over a frequency range from 50 Hz to 10 kHz. Because of the large dynamic ranges involved an automatic gain control is used to maintain a nearly constant output signal amplitude. The time constant of the automatic gain control is 0.5 sec. Second, a 16-channel spectrum analyzer is used to provide absolute measurements of the voltage spectral densities of the received signals over the frequency range from 10 Hz to 56 kHz. The scan time of the 16-channel spectrum analyzer is 4 sec and the averaging time constant is approximately 50 msec. For a further description of the plasma wave instrument, see Scarf and Gurnett [1977].

The Voyager 2 trajectory by Uranus is shown in Figure 2. Because the rotational axis of Uranus was nearly parallel to the planet-sun

line at the time of encounter, the spacecraft approached from the sunlit (south) pole of the planet, passed through the equatorial plane, and then departed over the dark (north) pole. The equatorial plane crossing occurred at 1715:26 SCET (spacecraft event time) on January 24, 1986, at a radial distance of 115,401 km (4.51 R_U, based on R_U = 25,600 km), slightly inside the orbit of Uranus' satellite Miranda. For purposes of describing the spacecraft position we use the Uranus-centered coordinate system adopted by the Voyager project for the Uranus flyby and described by Cesarone et al. [1984]. The only exception is that we use the IAU convention regarding the direction of the poles. In this system the +z axis is parallel to the rotational axis and directed toward the north (dark) pole as illustrated in Figure 2. At the equatorial plane crossing (z = 0) the velocity components normal and parallel to the equatorial plane were U_z = 16.4 km/sec and U_o = 7.0 km/sec.

The dust impact noise was first detected in the 16-channel spectrum analyzer data at about 1712:30 SCET. The noise gradually increased in intensity over a few-minute period, reached maximum intensity at about 1716:06 SCET, shortly after the equatorial plane crossing, and then dropped back below the instrument noise level by about 1721:00 SCET. The antenna voltage variations from the 16-channel spectrum analyzer during this period are shown in Figure 3. As can be seen, the noise is very irregular and spiky, particularly near the beginning and end of the event. The intensity decreases rapidly with increasing frequency and drops below the instrument noise level at frequencies above about 5.62 kHz. At peak intensity the root-mean-square (rms) voltage integrated across all channels is 27.7 millivolts.

Confirmation that the noise is caused by particle impacts is provided by the broadband waveform data. Three 48-second frames of waveform data were taken from 1715:12 to 1717:36 SCET, centered on the nominal position of the equator crossing. When played through a speaker these signals sound like a "hailstorm," very similar to the particle impacts detected at Saturn's ring plane crossing [Scarf et al., 1982]. Plots of the voltage waveform show that the noise consists of hundreds of pulses, each lasting a few milliseconds. The impact rate, averaged over 12 sec intervals, reached a peak of 54.2 impacts/sec at 1715:42 SCET. Four representative samples of the waveform are shown in Figure 4. Typically the impact signal consists of a step-function-like increase, indicated by the arrows, followed by an oscillatory recovery phase lasting from one to several milliseconds. The rise time of the initial step is about 30 μsec, which corresponds roughly to the rise time expected from the upper cutoff frequency of the receiver, which is ~ 10 kHz. Therefore, the rise time is determined by the instrument response. The pulse amplitudes vary over a wide range. Some of the pulses, such as in panel (a) are small and within the dynamic range of the waveform receiver, whereas other pulses, such as in panels (c) and (d) are large and severely clipped. The strongly clipped pulses usually have a very complex oscillatory waveform during the recovery phase. This complex behavior is believed to be caused by receiver distortion effects and is almost certainly not representative of the actual waveform on the antenna. The true waveform is probably best represented by unclipped pulses, such as in

panels (a) and (b). These waveforms usually consist of an initial pulse of one polarity, typically lasting a fraction of a millisecond, followed by a longer recovery pulse of lower amplitude and opposite polarity. As can be seen in Figure 4, the polarity of the initial pulse can be either positive or negative. Positive and negative polarities occur with about equal probabilities. The ratio of the number of positive to the number of negative pulses is 0.829 ± 0.02.

The broadband waveform signals can also be Fourier transformed to produce a spectrum, several representative examples of which are shown in Figure 5. Because the automatic gain control destroys amplitude information, only relative amplitudes are shown. At high frequencies the voltage spectral density, $V^2/\Delta f$, decreases with increasing frequency, varying approximately as f^{-2}. The f^{-2} spectrum is believed to be caused by the clipped square-wave-like waveform, which at high frequencies would produce a f^{-2} power spectrum, and is not representative of the true spectrum. At low frequencies a distinct break occurs in the spectrum at about 300 Hz, with a tendency to flatten at low frequencies. This feature is believed to be mainly due to the shape of the recovery waveform, which is dominated by frequency components in this range. Comparisons to the Saturn observations summarized by Gurnett et al. [1983] show that the waveforms and spectrums are very similar to the impacts detected at Saturn's ring plane crossing.

III. COUPLING MECHANISM

In order to interpret these observations, we now discuss the mechanisms by which the kinetic energy of an impacting particle can be converted into an electrical signal. Since no damage is known to have occurred to the spacecraft electronics or instruments, the particles must be quite small. Laboratory tests show that at a velocity of 20 km/sec a particle with a radius of 100 μm can penetrate several millimeters of aluminum [Frost, 1970], which is comparable to the thickness of the outer skin of the spacecraft. Therefore, it seems certain that the particles have a radius less than 100 μm. Only three mechanisms are known by which such small particles can produce electrical signals. These mechanisms are (1) direct detection of charge on the particle, (2) microphonics, and (3) impact ionization. In the analysis of the impact noise observed at Saturn's ring plane, Gurnett et al. [1983] concluded that only impact ionization can produce the observed pulse amplitudes. Since the impact noise detected at Uranus is essentially the same as at Saturn, we will assume without further argument that the noise is produced by impact ionization.

Impact ionization is basically a simple process. When a small particle strikes a solid surface at a sufficiently high velocity, the particle, together with some of the surface material, is vaporized and heated to an extremely high temperature, $\sim 10^5$°K [Hornung and Drapatz,

1981]. Because of the high temperature, some of the gas is ionized, thereby producing a small cloud of plasma that expands away from the impact site, as illustrated in Figure 6. The amount of charge released has been studied by several investigators, including Friichtenicht [1964], Auer and Sitte [1968], Adams and Smith [1971], Dietzel et al. [1973], McDonnell [1978], Fechtig et al. [1978], and Grün [1984]. These studies show that to a good approximation the charge Q released is proportional to the mass m of the particle,

$$Q = km, \tag{1}$$

where k is a yield constant that depends on both the speed of the particle and the composition of the particle and the target. The yield constant is estimated by taking the value used for analyzing the impacts at Saturn, which was 0.21 C/gm [Gurnett et al., 1983], and correcting for the higher impact velocity at Uranus using a velocity cubed scaling law [see Grün, 1984]. For particles in equatorial circular orbits, revolving in the same direction as Uranus' rotation, the relative speed between the spacecraft and the particles is U = 20.4 km/sec. The corresponding speed at Saturn was 13.8 km/sec, which gives a correction factor of 3.23, and a yield constant of k = 0.70 C/gm. This yield constant is representative of a dielectric particle (ice) striking a metal surface (aluminum) and could easily vary by as much as a factor of 10 depending on the particle composition and structure.

Next, we consider the coupling of the charge pulse to the electric antenna. From similar observations at Saturn's ring plane, it is known that the impacts detected are primarily from the spacecraft body and not the antennas [Gurnett et al., 1983]. This conclusion is based on a comparison of the projected area of the two antenna elements and the ratio of the number of positive to the number of negative pulses. Since the receiving system responds to the voltage difference between the two elements, if the impacts were primarily on the antennas then the ratio of positive to negative pulses should correspond to the ratio of the projected areas. For the Saturn ring plane crossing the ratio of the projected antenna areas was $A_1/A_2 = 1.82$. The ratio of the number of positive pulses to the number of negative pulses was $R_+/R_- = 1.13 \pm 0.01$. Since the ratio of positive to negative pulses does not correspond to the antenna area ratio, we concluded that the impacts must be mainly on the spacecraft body. A comparable test cannot be performed at Uranus. As it turns out, for Uranus, the direction of arrival of the particles in the spacecraft frame of reference is very close to the y_{sc}-z_{sc} plane, $\vec{U}$ = (4.75, 8.51, 17.9) km/sec, which makes the ratio of projected areas (see Figure 1) very close to unity. For this geometry impacts on both the antenna and the spacecraft body should give almost the same number of positive and negative pulses, so the two types of impacts cannot be distinguished. Since it appears that the impact process is essentially the same at Saturn and Uranus, we will assume that the impacts detected at Uranus are primarily on the spacecraft body.

For impacts on the spacecraft body, there are two mechanisms for converting the charge to a voltage pulse out of the receiver. In the first mechanism, called the antenna collection model, it is assumed that the voltage pulse is caused by charge collection on the antennas. Since it is very unlikely that an impact will occur symmetrically with respect to the two antennas, the charge collected by one of the antennas will probably be substantially larger than the charge collected by the other antenna. The receiver output will then be dominated by the element that collects the largest charge. In this case the amplitude of the voltage pulse out of the receiver can be written

$$V = \alpha \frac{Q}{C_A} \quad , \tag{2}$$

where α is a collection coefficient and C_A is the antenna capacitance (including base capacity). For Voyager, the antenna capacity is $C_A \approx$ 90 pf. The antenna collection model was used by Gurnett et al. [1983] to analyze the impacts observed during the Saturn ring plane crossing. The main problem with this model is the difficulty of estimating the collection coefficient α. Because of the fast rise time of the voltage pulse, it appears that the charge collected by the antenna is mainly due to electrons. It is easily verified that for the high temperatures expected during the expansion phase [Hornung and Drapatz, 1981] the transit time for ions to travel from the spacecraft to the antenna is too long (typically a few milliseconds) to account for the

observed rise times. From simple geometric considerations it would appear that the collection coefficient should be very small, since the solid angle of the antenna is quite small as viewed from a typical impact site. However, because the antenna should have a positive bias voltage due to photoelectron emission, the efficiency for collecting electrons is probably larger than would be estimated from simple geometric considerations. Arguments were presented by Gurnett et al. [1983] suggesting that the collection coefficient was in the range from 0.1 to 1.0, but the method used for estimating α (based on the R_+/R_- ratio) was highly uncertain and subject to substantial errors.

In the second mechanism, called the spacecraft collection model, it is assumed that the receiver responds to the charge collected by the spacecraft body. Because the plasma cloud is formed very close to the surface the spacecraft body should be a very efficient collector. In fact, laboratory experiments sometimes use measurements of the charge deposited on the target to estimate the total charge yield [Grün, 1984]. If most of the charge is collected, a voltage pulse is produced on the spacecraft body with an amplitude given by Q/C_{sc}, where C_{sc} is the spacecraft capacitance. For Voyager C_{sc} is mainly determined by the magnetometer boom and is estimated to be about 330 pf. Ideally, for a differential measurement the plasma wave receiver should not respond to a voltage pulse on the spacecraft body. However, because of imbalances in the antenna and differential amplifier, a response can occur. The amplitude of the voltage pulse out of the receiver can be written

$$V = \gamma \frac{Q}{C_{sc}} \quad , \tag{3}$$

where γ is a constant called the common mode rejection. Based on the preflight calibrations, the common mode rejection is believed to be about $\gamma \simeq 3 \times 10^{-3}$.

Of the two models, we believe that the antenna collection mechanism provides the best model for analyzing the response of the plasma wave instrument to particle impacts. Strong evidence exists that the plasma wave instrument does not respond to charge collection by the spacecraft body. One of the characteristics of a common mode response is that the voltage pulses should all be of the same sign. The sign depends on the sign of the common mode imbalance. Since the pulses are observed to have an equal number of positive and negative polarities, charge collection by the spacecraft body produces a negligible contribution to the observed pulse amplitude. The absence of a detectable common mode response allows us to put a limit on the antenna collection coefficient. Since the voltage given by Equation 2 must be much larger than the voltage given by Equation 3, it follows that

$$\alpha \frac{Q}{C_A} >> \gamma \frac{Q}{C_{sc}} \quad , \tag{4}$$

or

$$\alpha >> \gamma \frac{C_A}{C_{sc}} \simeq 8.2 \times 10^{-4} \quad . \tag{5}$$

Since α cannot exceed one, the antenna collection coefficient is bounded by the following limits

$$8.2 \times 10^{-4} << \alpha \leq 1 \quad . \tag{6}$$

Because of the broad range of these limits, this inequality is not particularly useful.

A better estimate of the antenna collection coefficient can be obtained by comparison with the Planetary Radio Astronomy (PRA) measurements given by Meyer-Vernet et al. [1986]. Because the radio astronomy instrument uses the antennas as monopoles, the PRA instrument has no common mode rejection ($\gamma = 1$) and responds directly to the charge collected on the spacecraft body. Equation 3 with $\gamma = 1$ then provides a direct determination of the pulse amplitude detected by the PRA instrument. The peak voltage spectral densities detected by the plasma wave (PWS) and PRA instruments are compared in Figure 7. Although the integration times and sample rates of the two instruments are not exactly the same (50 msec and 1 sample/4 sec for PWS and 25 msec and 1 sample/6 sec for PRA) these differences are not large enough to cause a significant different in the peak intensities. Although the general form and slope of the spectrums are very similar, the PWS intensities are seen to be much lower than the PRA intensities. The offset in the voltage spectrum is approximately $V_{PWS}/V_{PRA} = 0.018$. A similar offset (not yet published) is also observed at the Saturn ring plane crossing. We attribute this offset to the difference in the antenna voltage response of the two instruments (dipole

versus monopole). Since the PRA monopole antenna responds directly to the total charge released, the offset provides a direct determination of the average charge collection coefficient of the PWS dipole antenna. Using Equation 2 for the PWS voltage and Equation 3 (with $\gamma = 1$) for the PRA voltage, one can write

$$V_{PWS} = 0.018 V_{PRA} \quad , \text{ or}$$

$$\alpha \frac{Q}{C_A} = 0.018 \frac{Q}{C_{sc}} \quad . \qquad (7)$$

After eliminating Q from both sides of the equation and substituting the nominal values for C_A and C_{sc} one obtains $\alpha = 4.8 \times 10^{-3}$. This value is within the limits given by Equation 6, and is therefore consistent with the fact that no common mode response is detected by the plasma wave experiment.

The collection coefficient derived above is considerably smaller than the collection coefficient used by Gurnett et al. [1983] in the analysis of the impacts at Saturn's ring plane crossing. We believed that the present estimate, $\alpha = 4.8 \times 10^{-3}$, is based on a better principle and is probably more reliable than the values used at Saturn. However, it still must be recognized that the collection coefficient is at best a rough estimate, and could still be in error by a substantial factor. Also, it should be noted that the collection coefficient represents an average over many impacts and is not applicable to any given impact since the actual collection coefficient depends in a complicated way on the exact location of the impact, which is unknown.

IV. NUMBER DENSITY AND PARTICLE MASS

Using the antenna coupling model described in the previous section we can now determine the number density and mass of the impacting particles. The number density, n, is determined by the equation

$$R = nUA_{sc} \quad , \tag{8}$$

where U is the relative speed between the spacecraft and the particles, A_{sc} is the effective area of the spacecraft body and R is the impact rate. As discussed earlier, the relative speed between the spacecraft and the particles is U = 20.4 km/sec. The effective area of the spacecraft has been estimated by Gurnett et al. [1983] for the Saturn particle impacts and is approximately A_{sc} = 1.66 m^2. Although the direction of arrival is different at Uranus, the projected area is relatively insensitive to the arrival direction and is assumed to be the same as at Saturn. The impact rate R has been computed by using an algorithm that searches for two successive slopes of the same sign exceeding a preset threshold. The threshold was adjusted to give good identification of events of the type shown in Figure 4. To avoid counting false events during the transient recovery phase, a dead time was introduced after each event. Since the receiver usually takes longer to recover after larger events, the dead time is increased for

events with larger slopes. The average dead time is about 1.6 msec. The impact rate determined from the waveform analysis is shown in Figure 8 as a function of the distance z from the equatorial plane. A Gaussian profile of the form

$$R = R_o \exp\left[\frac{-(z - z_o)^2}{\Delta z^2}\right] , \qquad (9)$$

is found to provide a good fit, where R_o is the maximum impact rate, z_o is the offset from the equatorial plane, and Δz is a measure of the thickness of the impact region. The best fit values are $R_o = 54.2 \pm 0.8$ sec^{-1}, $z_o = 280 \pm 29$ km, and $\Delta z = 1740 \pm 66$ km.

Using Equation 8, the impact rate has been replotted and converted to a number density in the top panel of Figure 9. The number density is shown by the scale on the right-hand side of the panel. The maximum number density is seen to be about 1.6×10^{-3} particles/m^3, which corresponds to a mean distance between particles of about 8.5 m. This number density should be relatively accurate since there is very little uncertainty in any of the parameters involved. The velocity U is known from simple geometric considerations to an accuracy much less than 1%, and the statistical uncertainty in the counting rate is only about 4%. The largest error is probably caused by the uncertainty in the effective area of the spacecraft. The effective area is believed to be accurate to about 10% to 20%, which means that the number density is known to a similar accuracy.

Next we consider the mass threshold for counting impacts in the waveform data. By combining Equations 1 and 2 the mass of the impacting particle can be computed from the amplitude of the voltage pulse on the antenna using the relation

$$m = \left(\frac{C_A}{\alpha k}\right) V \quad . \tag{10}$$

Since the gain of the waveform channel is continuously adjusted by the automatic gain control to maintain a constant rms output voltage, the threshold voltage, V*, for detecting an impact is directly proportional to the rms antenna voltage, V_{rms},

$$V^* = \beta V_{rms} \quad . \tag{11}$$

The proportionality constant β has been previously evaluated by Gurnett et al. [1983] and is approximately $\beta = 0.51$. Combining Equation 11 with Equation 10 gives the following relation for the mass detection threshold

$$m^* = \left(\frac{\beta C_A}{\alpha k}\right) V_{rms} \quad . \tag{12}$$

The rms antenna voltage can be computed from the 16-channel spectrum analyzer data and is shown in the bottom panel of Figure 9. A scale on the right-hand side shows the corresponding mass threshold, m*, computed from Equation 12 using the nominal values for k, α, β and C_A.

From this plot it is seen that at the time of maximum impact rate, the mass threshold for counting impacts is about 4.5×10^{-10} gm. For a mass density of 1 gm/cm^{-3}, which would be representative of a typical dielectric particle (ice, for example), the corresponding radius for a spherical particle would be about 4 μm. More dense particles, such as silicates, would have somewhat smaller radii. Note that since the radius varies as the cube root of the mass the size of the particle is relatively insensitive to parameters such as α and k. Therefore, even with the uncertainties in these parameters, the radii must be on the order of a few microns. This conclusion is consistent with the conclusions of Meyer-Vernet et al. [1986] who based their estimates on related but somewhat different considerations.

A more quantitative estimate of the particle mass can be obtained directly from the rms antenna voltage. As a simple model we assume that the waveforms consist of rectangular pulses of amplitude V_n and duration τ_n. Using Equation 10, the rms antenna voltage averaged over time T can be written

$$V_{rms}^2 = \frac{1}{T} \sum_n V_n^2 \tau_n = \left(\frac{\alpha k}{C_A}\right)^2 \frac{1}{T} \sum m_n^2 \tau_n \quad . \tag{13}$$

Although the pulse durations vary somewhat, these variations are small compared to the amplitude variations. Therefore, the pulse duration can be taken to be a constant $\tau_n = \tau$. The time interval T can be re-expressed in terms of the total number of impacts N using the relation N = RT, so that

$$V_{rms}^2 = \left(\frac{\alpha k}{C_A}\right)^2 R\tau \left[\frac{1}{N} \Sigma m_n^2\right] \quad . \tag{14}$$

The quantity in brackets on the right is just the rms mass squared, m_{rms}^2. The rms mass is therefore directly related to the rms antenna voltage. The corresponding equation is

$$m_{rms} = \left(\frac{C_A}{\alpha k}\right) \frac{1}{\sqrt{R\tau}} V_{rms} \quad . \tag{15}$$

At the point of maximum impact rate, R = 54.2 sec^{-1}, the rms antenna voltage was 23.0 mV. Using τ = 1 msec, and the nominal values for the remaining parameters the rms mass works out to be $m_{rms} = 2.6 \times 10^{-9}$ gm. For a spherical particle with a density of 1 gm cm^{-3} the corresponding radius is 8.5 μm. Since small particles, less than $m^* \simeq 4.5 \times 10^{-10}$ gm are not counted, the rms mass may be overestimated to some extent.

It is evident from Figure 9 that the rms antenna voltage has a much larger level of fluctuations than the impact rate. Although the spiky features in the V_{rms} plot could be due to structure in the spatial distribution, we believe that it is more likely that the variations are due to statistical fluctuations. Since the sample rate of the 16-channel spectrum analyzer (1 sample/4 sec) is much lower than the sample rate of the waveform channel (28,800 samples/sec), the statistical fluctuations in V_{rms} are much larger than the fluctuations

in R. Rough estimates indicate that $\delta V_{rms}/V_{rms}$ should be about fifteen times $\delta R/R$, which agrees reasonably well with the observed fluctuation levels. Also, R includes all particles of mass greater than m*, whereas V_{rms} is biased toward the less numerous larger mass particles, which would further increase the fluctuations in V_{rms}. Two features which stand out that may not be statistical fluctuations are the abrupt steps up at 1714:40 and down at 1716:55, forming shoulders on a relatively flat region centered on the time of maximum impact rate. The symmetric location of these steps suggests that these features may be real.

V. DISCUSSION

This analysis shows that the particle impacts detected by the Voyager 2 plasma wave instrument at Uranus are caused by micron-sized particles. The mass threshold for detecting these particles is about $m^* \simeq 4.5 \times 10^{-10}$ gm, and the rms mass of the particles is estimated to be $m_{rms} = 2.6 \times 10^{-9}$ gm. The maximum number density is estimated to be about $n_o \simeq 1.6 \times 10^{-3}$ particles m^{-3}, and the north-south thickness of the impact region, based on a Gaussian fit, is $2\Delta z = 3480$ km. The maximum number density occurs after the equatorial plane crossing at a distance $z_o = +280$ km from the equatorial plane.

To check the overall consistency of these observations, it is useful to make a rough estimate of the geometric opacity and compare it with other observations. No particles or ring features were reported by the imaging team at the radial distance where Voyager crossed the equatorial plane [Smith et al., 1986]. Using the best fit Gaussian density profile, the columnar density normal to the equatorial plane is $\pi n_o \Delta z = 2.78 \times 10^3$ particles/m^2. If we assume that the particles all have a radius of $r_o = 8.5$ μm, the cross-sectional area per particle is $A_o = 2.2 \times 10^{-10}$ m^2. The geometric optical depth (assuming an optical efficiency of unity) is then approximately $\tau = \pi n_o A_o \Delta z = 6.3 \times 10^{-7}$.

To compare the geometric optical department with the limits imposed by the imaging system we must consider the illumination and viewing geometry. The Voyager approach to Uranus (nearly pole-on) presented a difficult situation for observing sheets of low optical depth material with the imaging system. The maximum sensitivity of the Voyager 2 wide angle camera (using the clear filter) produces a noise-level response from a target having reflectivity of about 10^{-4} of that of a perfect Lambert diffuser. The reflectivity ρ may be expressed in terms of the optical depth τ of a layer of particles as

$$\rho = \tau a P(\alpha)/4\cos(\varepsilon) \quad , \tag{16}$$

where a is the particle single-scattering albedo, $P(\alpha)$ is the phase function at phase angle α, and ε is the viewing angle measured from the normal to the layer (see e.g., Cuzzi et al. [1984]). There are three separate viewing geometries; pre-encounter with $\alpha \sim 30°$ and $\varepsilon \sim 0°$, ring plane crossing with $\alpha \sim 90°$ and $\varepsilon \sim 89°$, and forward scattering with $\alpha \sim 150°$ and $\varepsilon \sim 0°$. Because microscopic particles are capable of strong forward scattering, it might be expected that their detection would be optimized at high phase angles. Unfortunately, the maximum phase angles attained in images of the radial regions of interest here are not sufficiently large to produce significant scattering enhancements. Even worse, nearly all "deep" exposures at high phase angles are fogged by light scattered into the camera optics, possibly by reflections off of bright areas on the spacecraft.

The above effects limit the sensitivity of these images to a detection threshold of $\rho \sim 3.5 \times 10^{-4}$. Because the phase function and albedo of a wide variety of microscopic particles of absorbing material are fairly well constrained at $\alpha \sim 0.5$ and $P(150°) \sim$ several, our detection threshold in this geometry is $\tau \sim$ few $\times 10^{-4}$. Similar observations in backscattering geometry are at least one order of magnitude less sensitive to scattering by either microscopic material (because of the diminished phase function), or hypothetical parent macroscopic material (because of the low albedo $\alpha \sim 0.03$ which characterizes the macroscopic ring particles [Cuzzi, 1985; Ockert et al., 1986]). One image obtained at the ring plane crossing has favorable geometry for detecting faint ring material, but the phase function is least favorable here for either macroscopic or microscopic particles. This image has an unusual background noise distribution; although future reduction may be able to extract more information from this single image, at the moment an upper limit of $\tau \sim 10^{-4}$ in microscopic particles and $\tau \sim$ several $\times 10^{-4}$ in macroscopic particles also applies here. In either case, the geometric optical depth estimated from the PWS data is at least two orders of magnitude below the imaging system's detection threshold, and is therefore consistent with the imaging data.

The optical depth can also be compared with the PRA impact noise analysis of Meyer-Vernet et al. [1986]. The geometric optical depth computed from the PWS data, $\tau = 6.3 \times 10^{-7}$, is nearly two orders of magnitude larger than the optical depth, $\tau \sim 10^{-8}$, estimated from the PRA data. Most of this discrepancy can be traced to the north-south

thickness of the impact region which Meyer-Vernet et al. estimate (on the basis of an exponential scale height) to be only 150 km, compared to our value of $2\Delta z$ = 3480 km. We believe that our determination of the north-south thickness is probably much more reliable since the high time resolution of the PWS waveform measurements gives much better statistical accuracy for determining the impact rate profile (see Figure 8) than can be obtained from the PRA measurements. Also, Meyer-Vernet et al. assume the particle radius to be 2μm, which is somewhat smaller than our value of 8.5 μm, thereby further reducing the optical depth.

Next, we consider the question of the origin of the particles. The particles must have been produced relatively recently because such small particles are destroyed quickly and, moreover, their orbits evolve rapidly [Burns et al., 1980, 1984, 1986; Morfill et al., 1980a, 1980b; Grün et al., 1984]. The principal causes of destruction are catastrophic shattering caused by collisions with interplanetary micrometeoroids, and sputtering by magnetospheric ions. The particle orbits evolve systematically due to the drag of the magnetospheric thermal plasma and perhaps the atmosphere. For each of these processes, the lifetimes are poorly constrained because various parameters are quite uncertain for the Uranian system; nevertheless, for all these mechanisms, lifetimes are brief when compared to the solar system's age.

Collisions with micrometeoroids destroy the particles by catastrophic shattering rather than by progressive erosion [Burns et al.,

1980]. Assuming that the number of interplanetary micrometeoroids near Uranus is like that near Saturn [Humes, 1980], as should be the case if the meteoroids are cometary in origin, a particle's lifetime against catastrophic breakup should be $T_c \approx 10^6$ (1μm/r)^2 years, where r is the particle radius [Burns et al., 1984, 1986]. Sputtering rates depend upon the particle's unknown composition and the incompletely-defined energetic particle spectra [Johnson et al., 1984]. Near and just outside Miranda's orbit, proton fluences at a few keV measured by Voyager were $\sim 10^5$ cm^{-2} sec^{-1} [Bridge et al., 1986] while at tens of keV they were $\sim 10^4$ cm^{-2} sec^{-1} [Krimigis et al., 1986]; however, the energetic radiation flux dropped sharply inward of Miranda's orbit in the region of interest. With the given fluences, sputtering lifetimes are 10^5 - 10^6 (r/μm) years for water or methane ice; impacts with thermal plasma and the extended atmosphere [Broadfoot et al., 1986] could shorten this lifetime somewhat.

The orbits of the particles evolve due to momentum transferred in collisions with the thermal plasma and with the extended neutral atmosphere, each of which rotates with the planet. These processes move particles away from synchronous orbit (3.15 R_U), which implies an outward transport for the particles detected by Voyager. Evolution times by plasma drag [Burns et al., 1984; Grün et al., 1984] can be estimated knowing the thermal plasma density, which was measured to be 2 protons cm^{-3} near the equatorial plane passage [Bridge et al., 1986]. Characteristic orbital expansion times are $\sim 10^4$ - 10^5 (r/μm) years. Close to the planet Broadfoot et al. [1986] have pointed out

that drag from the extended Uranian exosphere will very effectively transport particles inward across the ring system. However, because of the steep decrease in the atmosphere's density with increasing height, atmospheric drag is not a significant factor in producing evolution of the particles detected by our instrument at 4.51 R_U. A final evolution mechanism, gyrophase drift, involves systematic drift toward synchronous orbit which may occur if the particles are highly charged [Northrop and Hill, 1983; Grün et al., 1984].

Given their young age, the particles detected by the plasma wave instrument must be continually generated, most likely by micrometeoroid impacts into parent bodies that, due to their larger size, can survive over the solar system's age. Since, as we have described above, the particle orbits evolve outward from synchronous orbit (3.15 R_U), the only plausible sources are 1985U1 (the largest of the small moons discovered by Voyager, at 3.28 R_U) or other unseen moonlets or small bodies that lie between 3.15 R_U and 4.51 R_U; the latter would be the Uranian counterparts of the moons believed to supply Jupiter's faint ring [Morfill et al., 1980b; Burns et al., 1980, 1984]. The locations of these objects relative to the Voyager trajectory are shown in Figure 10.

Because collisions, which cause flattening, occur infrequently in the tenuous rings, such systems are thicker than the main Saturnian and Uranian rings. The vertical extent of the Uranian dust layer ($2\Lambda z \approx$ 3480 km) is similar to that seen for the Saturnian material detected near the G ring by Pioneer's beer-can penetration experiment [Humes,

1980] and by Voyager's PRA and PWS instruments [Gurnett et al., 1983; Aubier et al., 1983]; the particles comprising Saturn's E ring as well as the Jovian halo are comparably elevated [Burns et al., 1984]. The thickness of these rings may have several causes. First, when the source objects lie on slightly inclined orbits (inclination i) at radius R, any particles that escape them with zero relative velocity will also travel along exactly the same trajectory. If these orbits spread through differential orbital precession (caused, for example, by radiation forces or non-point mass gravity coupled with some ring width), an azimuthally symmetric band of half thickness $\Delta z = Ri$ will develop. A half thickness of 1000 km requires inclinations of 0.5° for the source bodies; for comparison, the moonlets discovered by Voyager have no detectable orbital inclination while Miranda's orbit is inclined at 4.22°. A ring produced in such a manner would have its material preferentially located at the maximum elevation (cf. Dermott et al. [1984], Sykes and Greenberg [1986] who describe a similar distribution for the IRAS solar system dust bands), whereas the particles we detect are most numerous in the center of the distribution. Second, a thickened ring can be generated as a result of the speed at which ejecta escape the source bodies even if the latter lie in the equatorial plane. Then the half thickness Δz is approximately the injection speed times one-fourth the orbital period: for Δz = 1740 km, v = 20 m sec^{-1}, a reasonable speed for ejecta that leave a small satellite (see Figure 17 and associated discussion of Burns et al. [1984]). A Gaussian profile seems plausible for the ejecta since they should have

a distribution of velocities and enter the complex from various directions. Lastly, non-equatorial velocities may be produced because of non-equatorial forces. Circumplanetary material is almost certain to be electrically charged and, if so, dust in its movement through the tilted Uranian magnetic dipole field will experience Lorentz forces that have components out of the equatorial plane [Schaffer and Burns, 1987]. For a nominal electrical potential Φ of -100 V, numerical integrations [L. E. Schaffer, personal communication, 1986] find typical displacements of 2000 km off the ring plane at 4.51 R_U for particles of radius r = 1 μm in a tilted and displaced dipole like the preliminary models of the Uranian field [Ness et al., 1986]. Since the Lorentz acceleration scales as $\Phi\ r^{-2}$, this mechanism provides an attractive means to account for the mean ring thickness as well as some highly elevated particles. However, particles of 4 μm radius (like those our model finds) will be much less influenced by electromagnetic forces. For typical planetary magnetospheres, the equilibrium particle potentials are estimated to equal the plasma temperature or a few times it [Mendis and Axford, 1974; Grün et al., 1984]. Bridge et al. [1986] measured a plasma temperature of 4 to 50 electron volts, so Φ should be 10-100 V; note that the Voyager spacecraft itself reached a potential of -400 V during solar occultation [Bridge et al., 1986]. Latitudinal excursions of particles due to electromagnetic forces are enhanced at 4.51 R_U because of the nearby presence of the 2/1 and 3/2 outer Lorentz resonances at 5 R_U and 4.2 R_U, respectively [Burns et al., 1985, 1986]. If the particles originate

closer to Uranus (such as at 1985U1) and evolve outward across the 3/2, 4/3, ... Lorentz resonances, the large vertical excursions produced at the resonances will persist [Schaffer and Burns, 1987; L. E. Schaffer, personal communication, 1986] and this may allow 4 μm radius particles to reach 2000 km.

The apparent offset of the plane of symmetry of the particle distribution from the Uranian equatorial plane deserves explanation, but beforehand we should indicate that this observation may be misleading. First, the ring plane's position is subject to some uncertainty. The Voyager ephemeris that we have used to describe the spacecraft position relative to the planet depends upon a planetary rotation pole position determined from ground-based observations of ring occultations made prior to April 1981 [Elliot and Nicholson, 1984]. The most recent pole position, which incorporates additional ground-based and Voyager occultations [P. D. Nicholson, personal communication, 1986], shifts the Uranian pole's right ascension by -0.026° (±0.003°) and its declination by -0.124° (±0.003°). At 4.51 R_U, these corrections displace the equatorial plane by 54 km and 257 km, respectively; the former moves the equatorial plane crossing earlier in time while the latter's influence should be less important since the spacecraft transitted the ring plane near the intersection of the new and old equatorial planes. A second explanation rests on the fact that the measurement merely shows that the maximum signal occurs after ring plane crossing. Hence, the observed "latitudinal" offset could also be a consequence of radial variations in particle

number density combined with the spacecraft's oblique trajectory (the spacecraft crossed the equatorial plane at an angle of 23° to the normal). While it would be surprising if small particles were radially localized, it is not out of the question.

Assuming the latitudinal shift is real, three possible explanations may be offered. First, an asymmetric distribution could be seen if the injection occurred recently, whether from an inclined source or through a directed injection of material. The second possibility concerns electromagnetic forces: theoretical analyses [Northrop and Hill, 1983], numerical simulations [Schaffer and Burns, 1987] illustrate that charged particles introduced on the equatorial plane and interacting with the rotating tilted magnetic dipole field will asymmetrically spread as an outgrowth of these initial conditions. However, if such particles suffer subsequent collisions or their orbits drift appreciably (particularly through Lorentz resonances), symmetry is established. The third possibility arises because the mean gravitational plane (the so-called Laplace plane) is in fact determined by the competition between the planet's oblateness and the gravitational effect of Miranda on its inclined orbit. In the region of interest, the maximum warp of the ring plane due to this effect, computed from Equation 35b of Burns et al. [1979], is about 60 km.

ACKNOWLEDGEMENTS

The authors would like to acknowledge very helpful discussions with P. D. Nicholson and L. E. Schaffer, and thank R. Poynter for providing the arrival velocity of the particles in spacecraft coordinates. The research at the University of Iowa was supported by contract 957723 with the Jet Propulsion Laboratory, grants NGL 16-001-043, NAGW-871 and NGL 16-001-002 with NASA Headquarters, and contract N00014-85-K-0404 with the Office of Naval Research. The research at TRW was supported by NASA through contract 954012 with the Jet Propulsion Laboratory. The research at Cornell was supported through NASA Headquarters by grant NAGW-310.

REFERENCES

Adams, N. G., and D. Smith, Studies of micro particle impact phenomena leading to the development of a highly sensitive micrometeoroid detector, Planet. Space Sci., 19, 195, 1971.

Aubier, M. G., N. Meyer-Vernet, and B. M. Pedersen, Shot noise from grain and particle impacts in Saturn's ring plane, Geophys. Res. Lett., 10, 5, 1983.

Auer, S., and K. Sitte, Detection technique for micrometeoroids using impact ionization, Earth Planet. Sci. Lett., 4, 178, 1968.

Bridge, H. S., et al., Plasma observations near Uranus: Initial results from Voyager 2, Science, 233, 89-93, 1986.

Broadfoot, A. L., et al., Ultraviolet spectrometer observations of Uranus, Science, 233, 74-79, 1986.

Burns, J. A., P. Hamill, J. N. Cuzzi, and R. H. Darisen, On the "thickness" of Saturn's rings caused by satellite and solar perturbations and by planetary precession, Astron. J., 1783, 1979.

Burns, J. A., M. R. Showalter, J. N. Cuzzi and J. B. Pollack, Physical processes in Jupiter's ring: Clues to its origin by Jove!, Icarus, 44, 339-360, 1980.

Burns, J. A., M. R. Showalter and G. E. Morfill, The ethereal rings of Jupiter and Saturn, Planetary Rings, ed. by R. Greenberg and A. Brahic, U. Arizona Press, Tucson, pp. 200-272, 1984.

Burns, J. A., L. E. Schaffer, R. J. Greenberg and M. R. Showalter, Lorentz resonances and the structure of Jupiter's ring, Nature, 316, 115-119, 1985.

Burns, J. A., L. E. Schaffer, J. N. Cuzzi and D. A. Gurnett, Dust in the Uranian system: Its origin and fate, Bull. Am. Astro. Soc., 18, 770-771, 1986.

Cesarone, R. J., A. B. Sergeyevsky, and D. L. Gray, Trajectory/ Navigation Data Package for Nominal Voyager 2 Uranus-System Flyby, JPL Interoffice Memorandum Voyager-NAV-84-42, Jet Propulsion Laboratory, Pasadena, CA, 1984.

Cuzzi, J. N., Rings of Uranus: Not so thick, not so black, Icarus, 63, 312-316, 1985.

Cuzzi, J. N., J. J. Lissauer, L. W. Esposito, J. B. Hollberg, E. A. Marouf, G. L. Tyler and A. Boiscot, Saturn's rings: Properties and processes, in Planetary Rings, ed. by R. Greenberg and A. Brahic, University of Arizona Press, Tucson, 1984.

Dermott, S. F., P. D. Nicholson, J. A. Burns and J. R. Houck, Origin of the solar system dust bands discovered by the IRAS, Nature, 312, 505-509, 1984.

Dietzel, H., G. Eichhorn, H. Fechtig, E. Grün, H. J. Hoffman, and J. Kissel, The HEOS 2 and Helios micrometeoroid experiments, J. Phys. E: Sci. Instrum., 6, 209, 1973.

Elliot, J. L., and P. D. Nicholson, The rings of Uranus, in Planetary Rings, ed. by R. Greenberg and A. Brahic, U. of Arizona Press, pp. 25-72, 1984.

Fechtig, H., E. Grün, and J. Kissel, Laboratory simulation, Cosmic Dust, ed. by J. A. M. McDonnell, Wiley, N. York, 1978.

Friichtenicht, J. F., Micrometeoroid simulation using nuclear acceleration techniques, Nucl. Instrum. Methods, 28, 70, 1964.

Frost, V. C., Meteoroid damage assessment, NASA Spec. Publ., 8042, 30, 1970.

Grün, E., Impact ionization from gold, aluminum, and PCB-Z, The Giotto Spacecraft Impact Induced Plasma Environment, ESA SP-224, 39, 1984.

Grün, E., G. E. Morfill and D. A. Mendis, Dust-magnetosphere interactions, Planetary Rings, ed. by R. Greenberg and A. Brahic, U. Arizona Press, Tucson, pp. 275-332, 1984.

Gurnett, D. A., T. F. Averkamp, F. L. Scarf, and E. Grün, Dust impacts detected near Giacobini-Zinner by the ICE plasma wave instrument, Geophys. Res. Lett., 13, 291, 1986b.

Gurnett, D. A., E. Grün, D. Gallagher, W. S. Kurth, and F. L. Scarf Micron-sized particles detected near Saturn by the Voyager plasma wave instrument, Icarus, 53, 236, 1983.

Gurnett, D. A., W. S. Kurth, F. L. Scarf, and R. L. Poynter, First plasma wave observations at Uranus, Science, 233, 106, 1986a.

Hornung, K., and S. Drapatz, Residual ionization after impact of large dust particles, The Comet Halley Probe Environment, ESA Report SP-155, Paris, 23, 1981.

Humes, D. H., Results of Pioneer 10 and 11 meteoroid experiments: Interplanetary and near-Saturn, J. Geophys. Res., 85, 5841-5852, 1980.

Johnson, R. E., L. J. Lanzerotti and W. L. Brown, Sputtering processes: Erosion and chemical change, Adv. Space Res., 4, 41-51, 1984.

Krimigis, S. M., T. P. Armstrong, W. I. Axford, A. F. Cheng, G. Gloeckler, D. C. Hamilton, E. P. Keath, L. J. Lanzerotti and

B. H. Mauk, The magnetosphere of Uranus: Hot plasma and radiation environment, Science, 233, 97-102, 1986.

McDonnell, J. A. M., Microparticle studies by space instruments, Cosmic Dust, ed. by J. A. M. McDonnell, Wiley, N. York, 1978.

Mendis, D. A., and W. I. Axford, Satellites and magnetospheres of the outer planets, Ann. Rev. Earth Planet. Sci., 2, 419, 1974.

Morfill, G. E., E. Grün and T. V. Johnson, Dust in Jupiter's magnetosphere: Physical processes, Planet. Space Sci., 28, 1087-1100, 1980.

Morfill, G. E., E. Grün and T. V. Johnson, Dust in Jupiter's magnetosphere: Origin of the ring, Planet. Space Sci., 28, 1101, 1980b.

Meyer-Vernet, N., M. G. Aubier, and B. M. Pedersen, Voyager 2 at Uranus: Grain impacts in the ring plane, Geophys. Res., Lett., 13, 617, 1986.

Ness, N. F., M. H. Acuña, K. W. Behannon, L. F. Burlaga, J. E. P. Connerney, R. P. Lepping and F. M. Neubauer, Magnetic fields at Uranus, Science, 85, 1986.

Northrop, T. G., and J. R. Hill, The adiabatic motion of charged dust grains in rotating magnetospheres, J. Geophys. Res., 88, 1, 1983.

Ockert, M. E., J. N. Cuzzi and C. C. Porco, Photometry of the Uranian rings, this issue.

Scarf, F. L., F. V. Coroniti, C. F. Kennel, D. A. Gurnett, W.-I. Ip, and E. J. Smith, Plasma wave observations at Comet Giacobini-Zinner, Science, 232, 377, 1986.

Scarf, F. L., and D. A. Gurnett, A plasma wave investigation for the Voyager mission, Space Sci. Rev., 21, 289, 1977.

Scarf, F. L., D. A. Gurnett, W. S. Kurth, and R. L. Poynter, Voyager 2 plasma wave observations at Saturn, Science, 215, 287, 1982.

Schaffer, L., and J. A. Burns, The dynamics of weakly charged dust: Motion through Jupiter's gravitational and magnetic fields, J. Geophys. Res., 92, in press, 1987.

Smith, B. A., et al., Voyager 2 in the Uranian System: Imaging science results, Science, 233, 43, 1986.

Sykes, M. V., and R. Greenberg, The formation and origin of the IRAS zodiacal dust bands as a consequence of single collisions between asteroids, Icarus, 65, 51-69, 1986.

Warwick, J. W., D. R. Evans, J. H. Romig, J. K. Alexander, M. D. Desch, M. L. Kaiser, M. Aubier, Y. Leblanc, A. Lecacheux, and B. M. Pedersen, Planetary radio astronomy observations from Voyager 2 near Saturn, Science, 215, 582, 1982.

FIGURE CAPTIONS

Fig. 1. A sketch of the Voyager spacecraft showing the mounting of the two antenna elements and the spacecraft coordinate system used in the analysis.

Fig. 2. The trajectory of the Voyager 2 spacecraft in the orbital plane. The spacecraft crossed the equatorial plane outside the visible ring system and inside the orbit of Miranda.

Fig. 3. The voltages measured by the 16-channel spectrum analyzer near the equatorial plane. The very intense broadband noise observed near the equator crossing ($z = 0$) is caused by particles hitting the spacecraft.

Fig. 4. A series of broadband waveforms of the particle impact noise. Note that both positive and negative polarities occur.

Fig. 5. Selected frequency spectrums of the broadband waveform data. The f^{-2} voltage spectrum is believed to be an instrumental effect caused by the square-wave-like waveform that occurs during the recovery phase (see Figure 4).

Fig. 6. A schematic illustration of the model used to analyze the voltage produced by an impact. Charge released by the impact is collected by the antenna, αQ, and by the spacecraft body, $-Q$. These charges produce voltage pulses of amplitudes $\alpha Q/C_A$ on the antenna and $-Q/C_{SC}$ on the spacecraft body. Because the plasma wave instrument operates as a differential system it does not respond to the voltage pulse on the spacecraft body.

Fig. 7. A comparison of the voltage spectrums detected by the plasma wave (PWS) and radio astronomy (PRA) instruments. The offset is believed to be caused by the different mode of electric field detection used by the two instruments (dipole for PWS and monopole for PRA).

Fig. 8. The impact rate R as a function of the distance z from the equatorial plane, and the best fit Gaussian profile (solid line).

Fig. 9. The impact rate R and rms antenna voltages V_{rms} can be analyzed to give the number density n and mass threshold m*. These quantities are shown by the scales on the right.

Fig. 10. The Voyager 2 trajectory relative to various objects that could be the source of the micron-sized particles. Since atomospheric and plasma drag cause the particles to evolve outward from synchronous orbit (3.15 R_U) the only possible sources are the satellite 1985U1, or other unseen small bodies that may lie between synchronous orbit and the Voyager equator crossing at 4.51 R_U.

C-G82-478-1

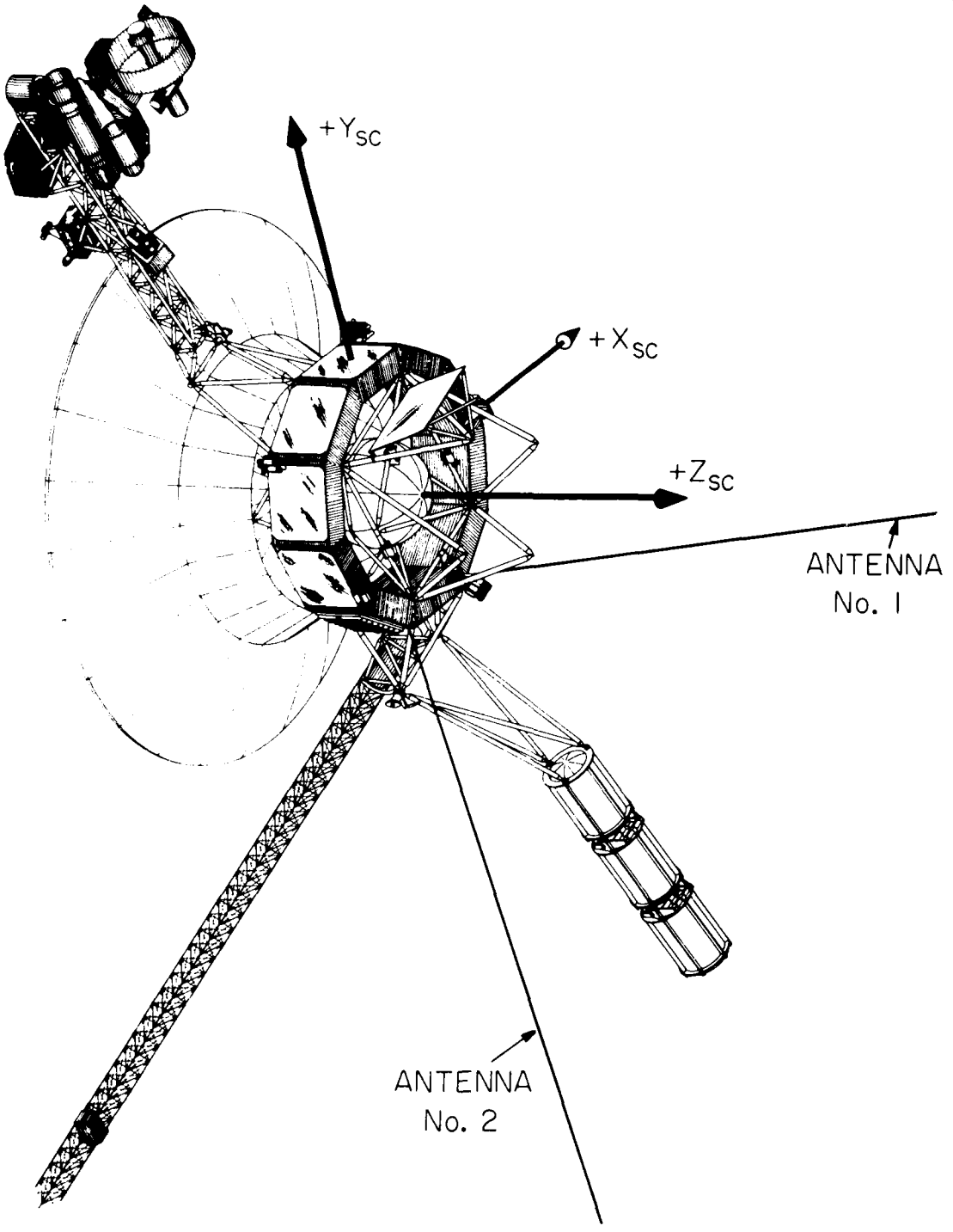

Figure 1

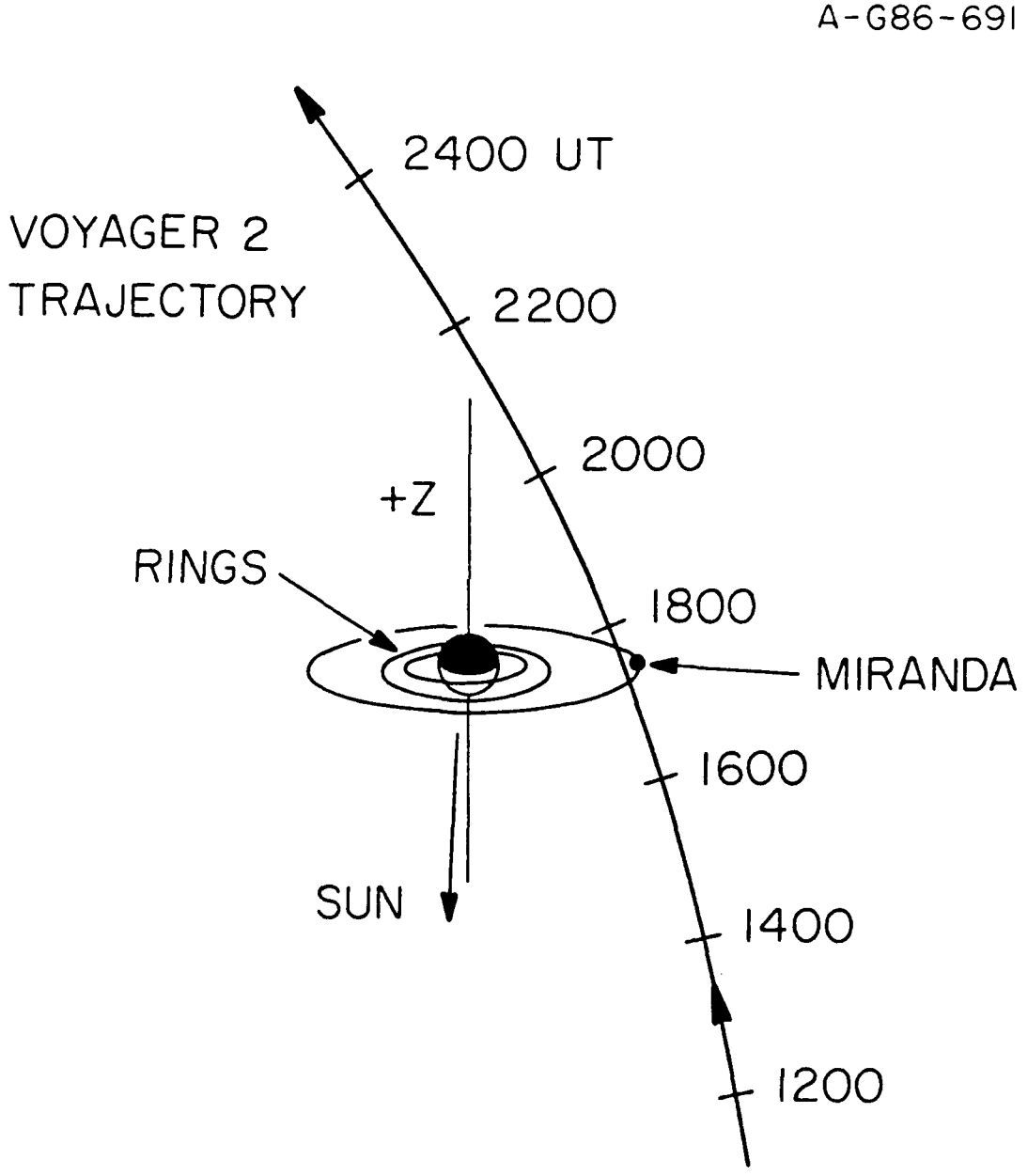
A-G86-691
2400 UT
VOYAGER 2
TRAJECTORY
2200
2000
+Z
RINGS
1800
MIRANDA
1600
SUN
1400
1200

Figure 2

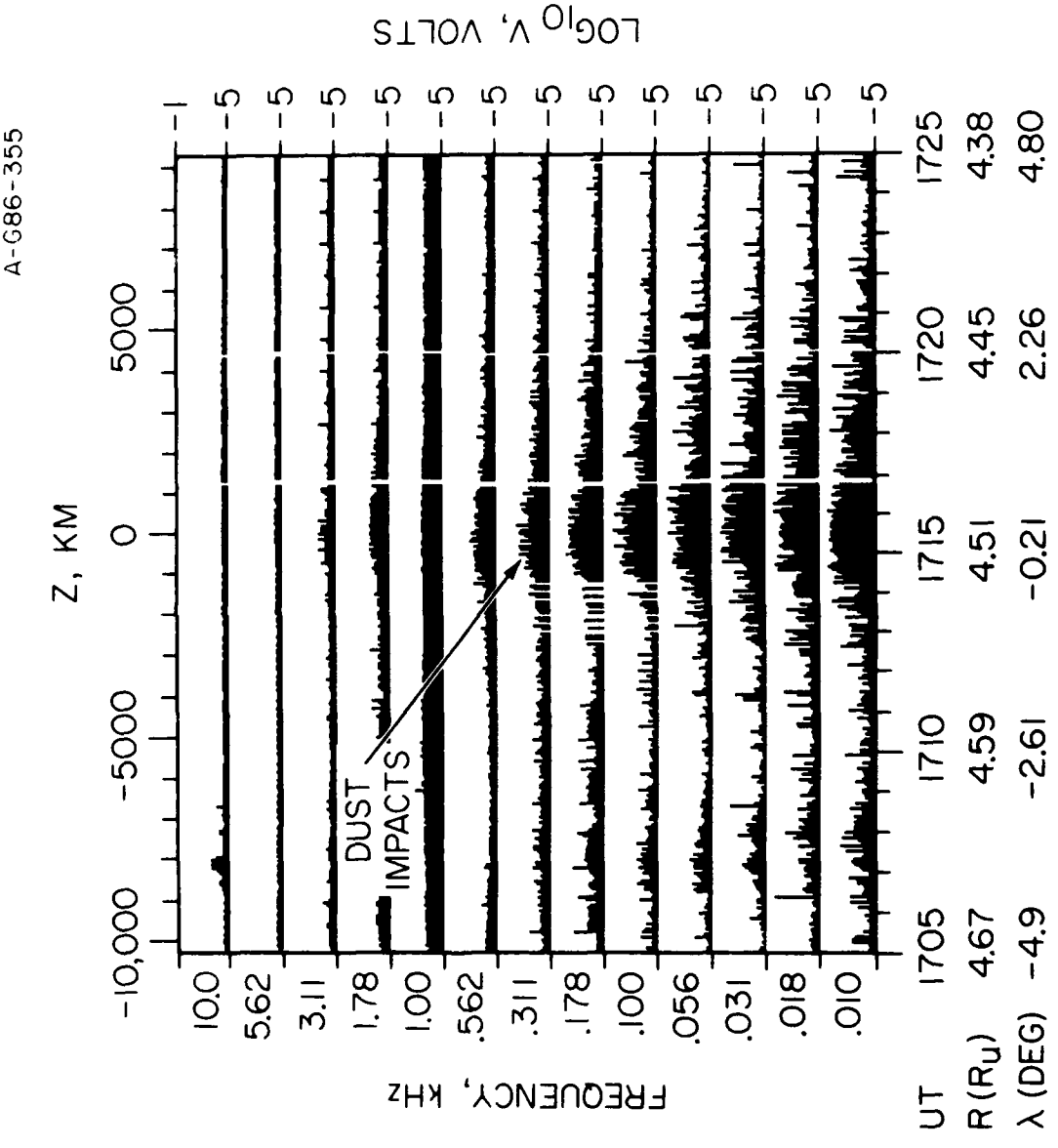
A-G86-355
LOG10 V, VOLTS
Z, KM
-10,000
-5000
0
5000
-1
-5
DUST
IMPACTS
FREQUENCY, kHz
10.0
5.62
3.11
1.78
1.00
.562
.311
.178
.100
.056
.031
.018
.010
UT 1705 1710 1715 1720 1725
R(RU) 4.67 4.59 4.51 4.45 4.38
λ (DEG) -4.9 -2.61 -0.21 2.26 4.80
VOYAGER 2, JAN. 24, 1986

Figure 3

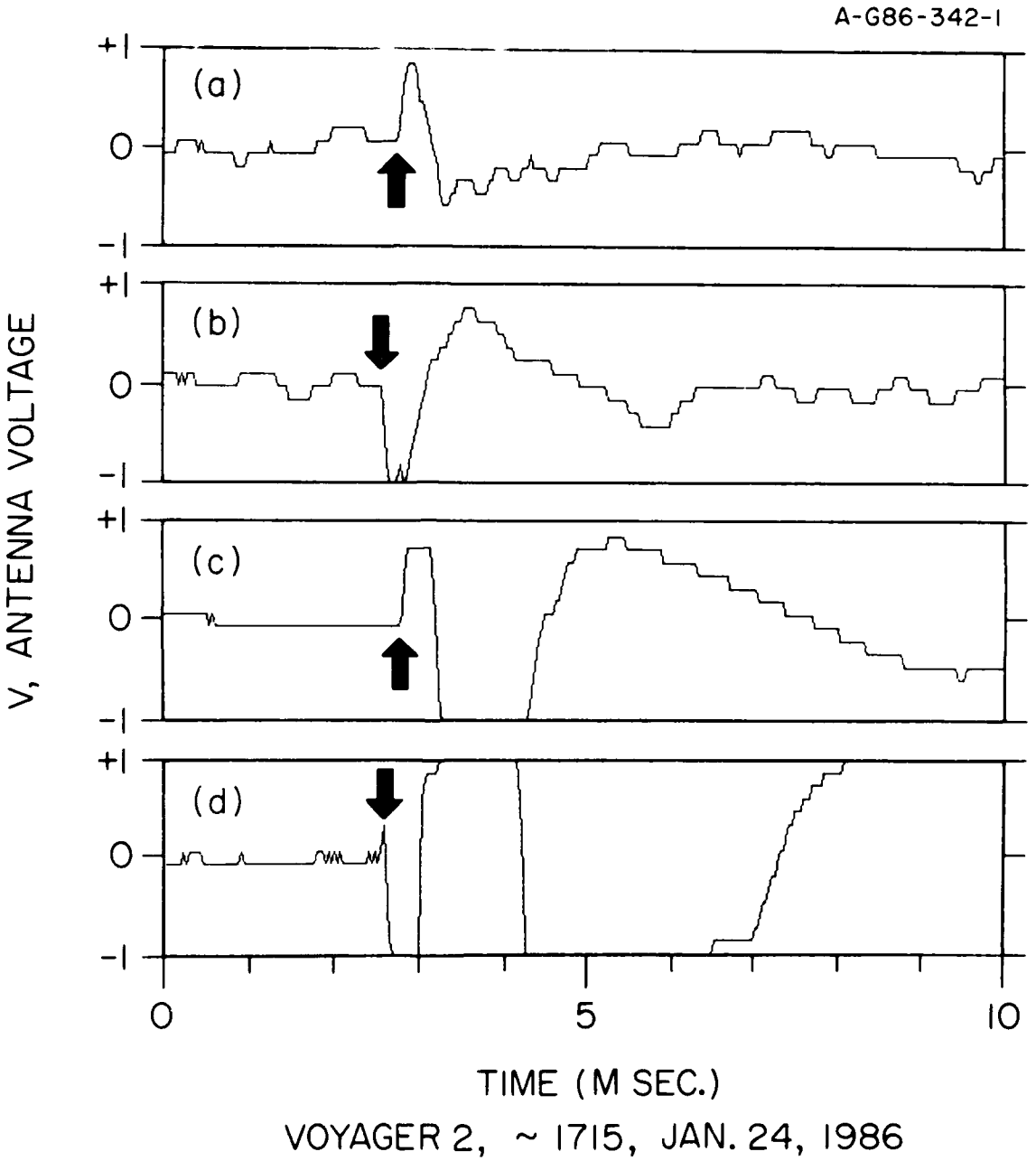
A-G86-342-1
+1
0
-1
(a)
(b)
(c)
(d)
V, ANTENNA VOLTAGE
0
5
10
TIME (M SEC.)
VOYAGER 2, ~ 1715, JAN. 24, 1986

Figure 4

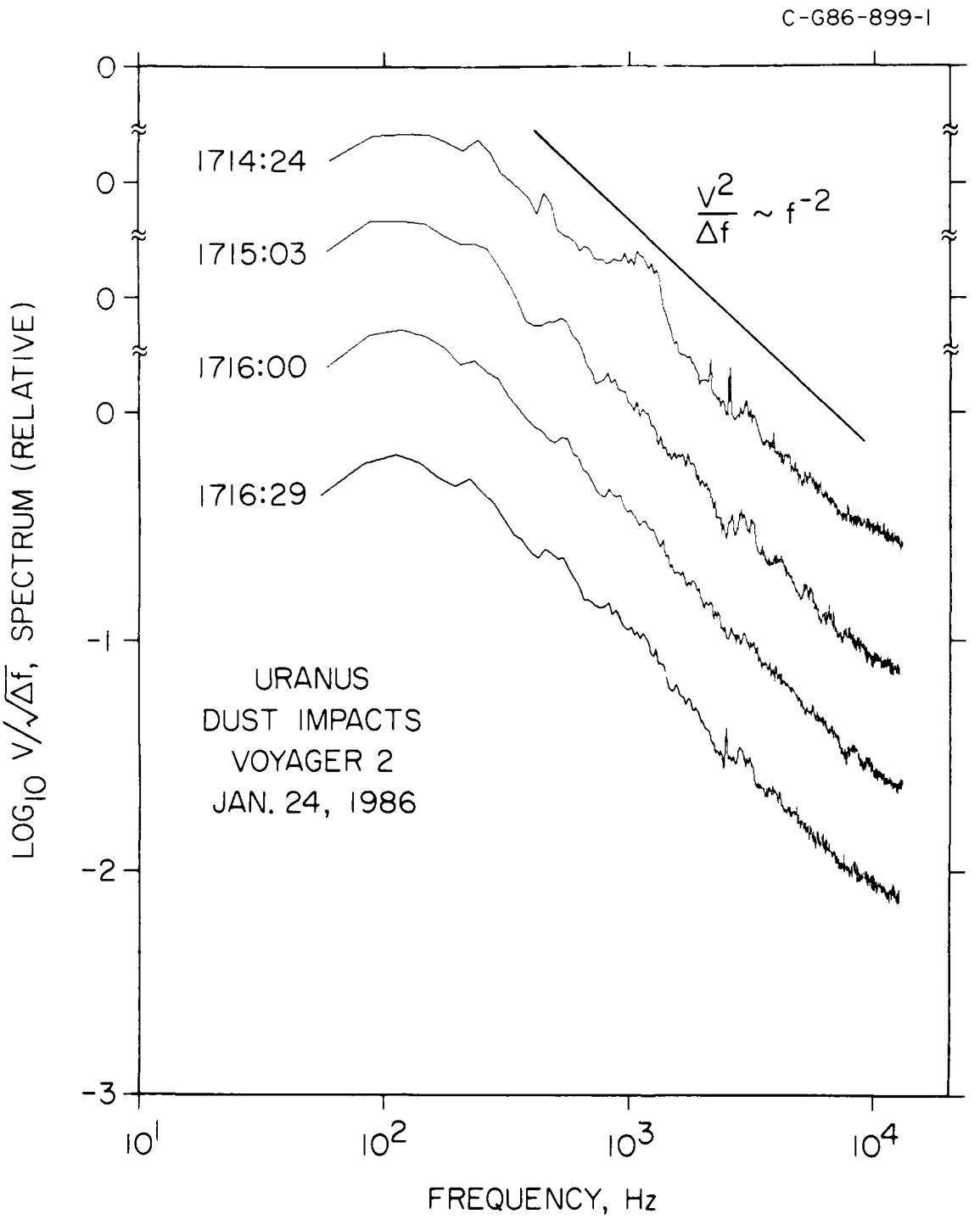
C-G86-899-1
1714:24
1715:03
1716:00
1716:29
$\frac{V^2}{\Delta f} \sim f^{-2}$
URANUS
DUST IMPACTS
VOYAGER 2
JAN. 24, 1986
LOG_{10} V/$\sqrt{\Delta f}$, SPECTRUM (RELATIVE)
FREQUENCY, Hz
0
0
0
0
-1
-2
-3
10^1
10^2
10^3
10^4

Figure 5

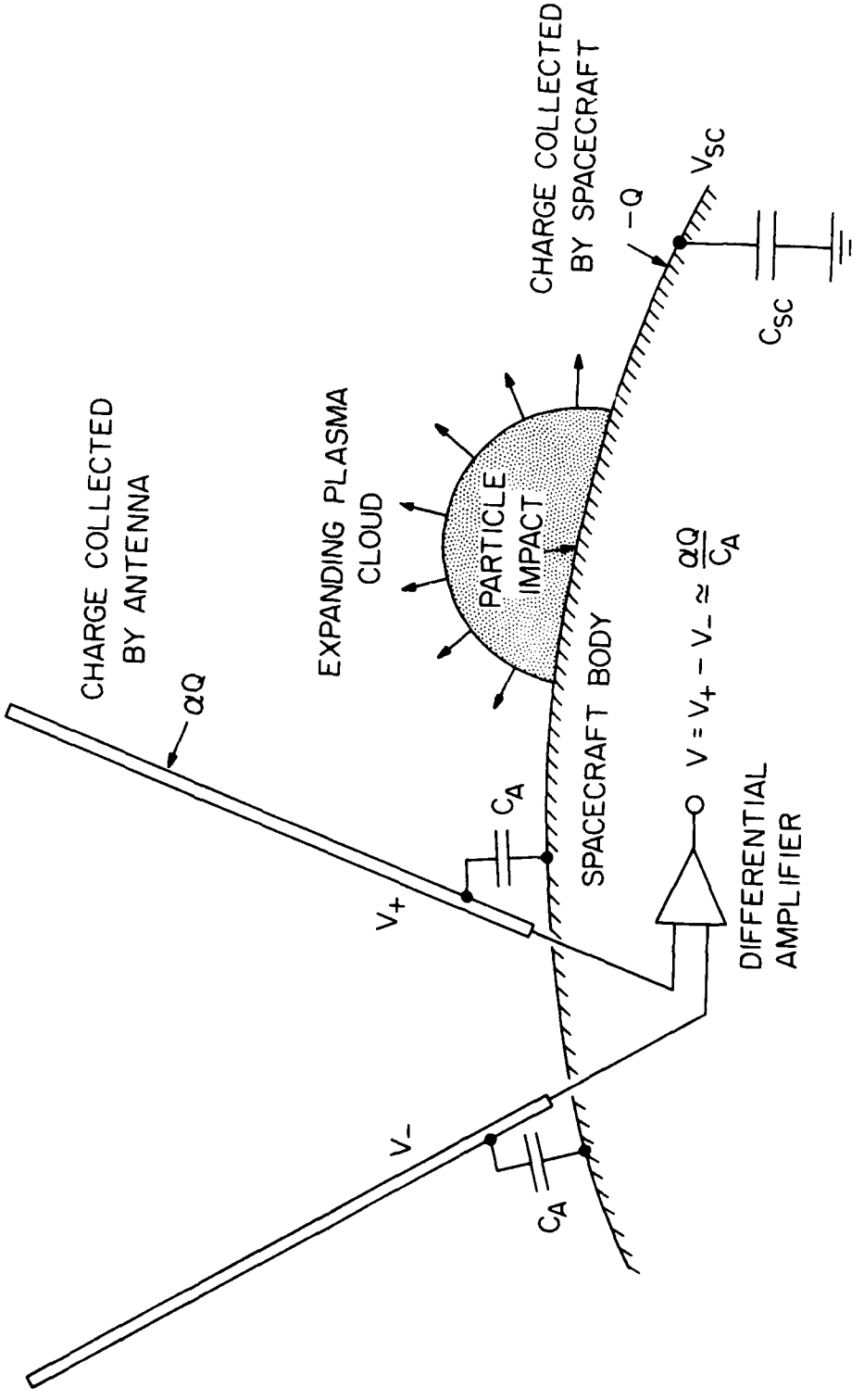
C-G86-807
CHARGE COLLECTED BY ANTENNA
αQ
EXPANDING PLASMA CLOUD
PARTICLE IMPACT
CHARGE COLLECTED BY SPACECRAFT
-Q
V_{SC}
C_{SC}
C_A
V_+
SPACECRAFT BODY
$V = V_+ - V_- \approx \frac{\alpha Q}{C_A}$
DIFFERENTIAL AMPLIFIER
V_-
C_A

Figure 6

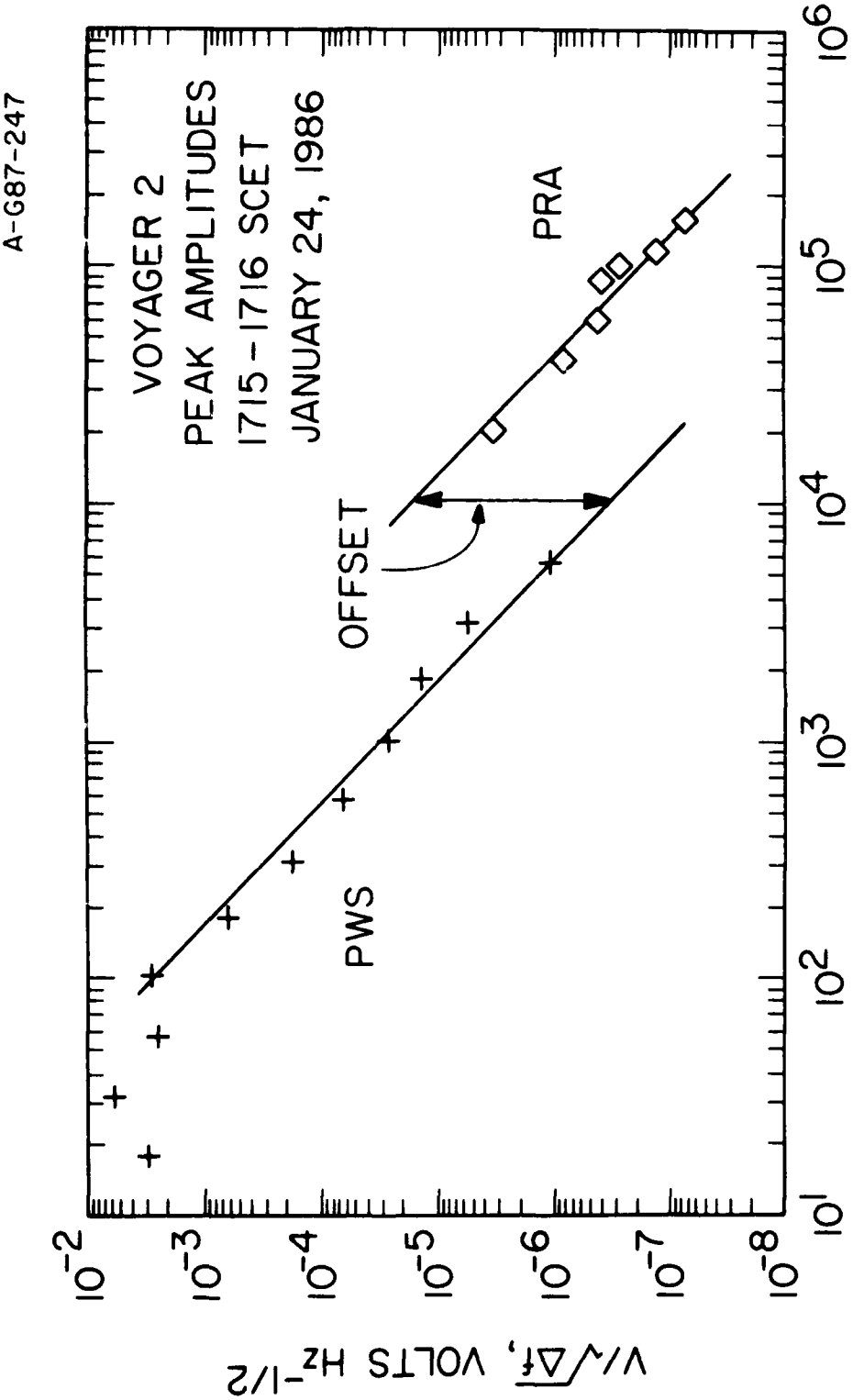
A-G87-247
VOYAGER 2
PEAK AMPLITUDES
1715-1716 SCET
JANUARY 24, 1986
PRA
OFFSET
PWS
V/√Δf, VOLTS Hz^-1/2
FREQUENCY, Hz
10^-2
10^-3
10^-4
10^-5
10^-6
10^-7
10^-8
10^1
10^2
10^3
10^4
10^5
10^6

Figure 7

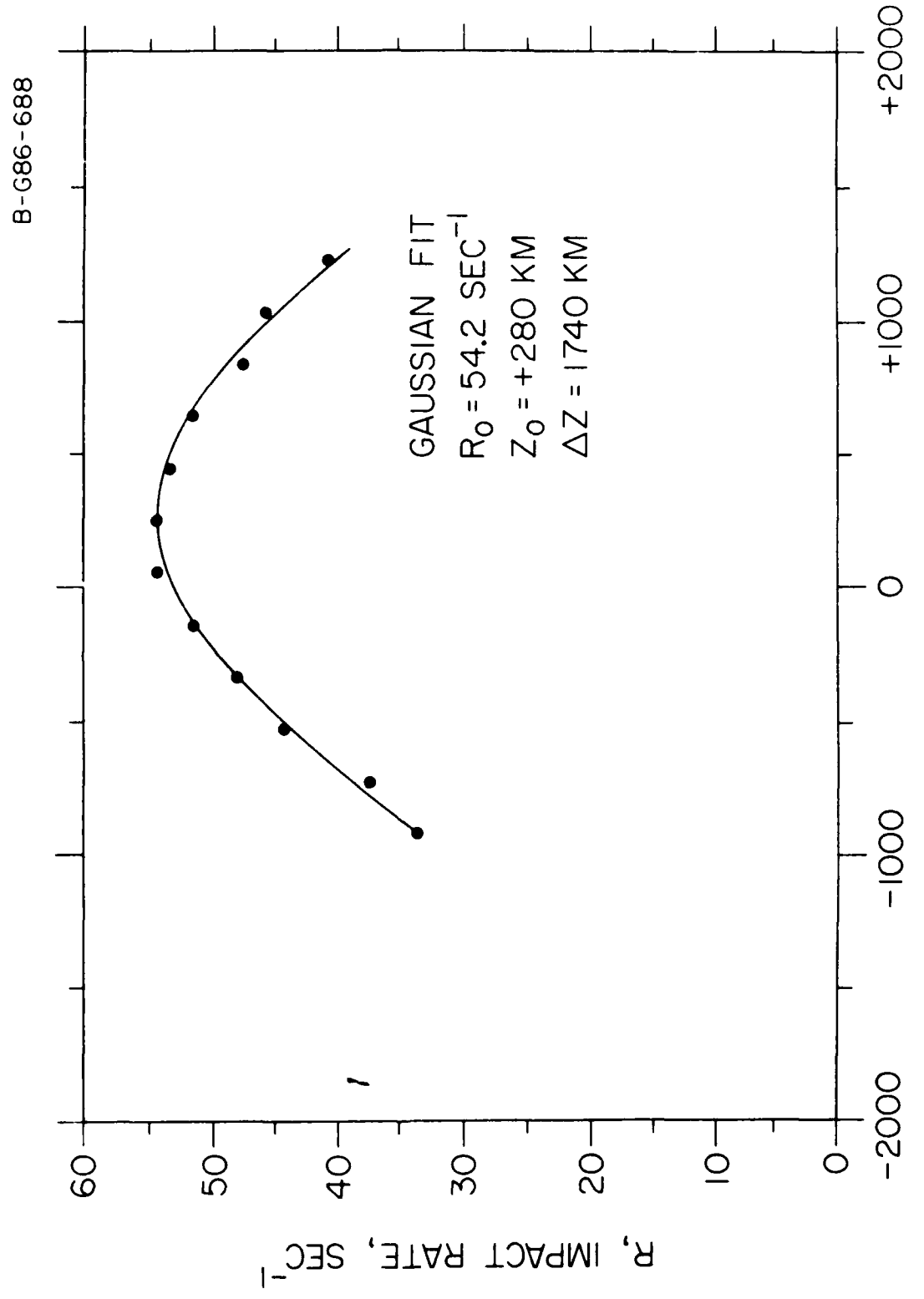
B-686-688
GAUSSIAN FIT
$R_0 = 54.2$ SEC^{-1}
$Z_0 = +280$ KM
$\Delta Z = 1740$ KM
R, IMPACT RATE, SEC^{-1}
Z, KM
60
50
40
30
20
10
0
-2000
-1000
0
+1000
+2000

Figure 8

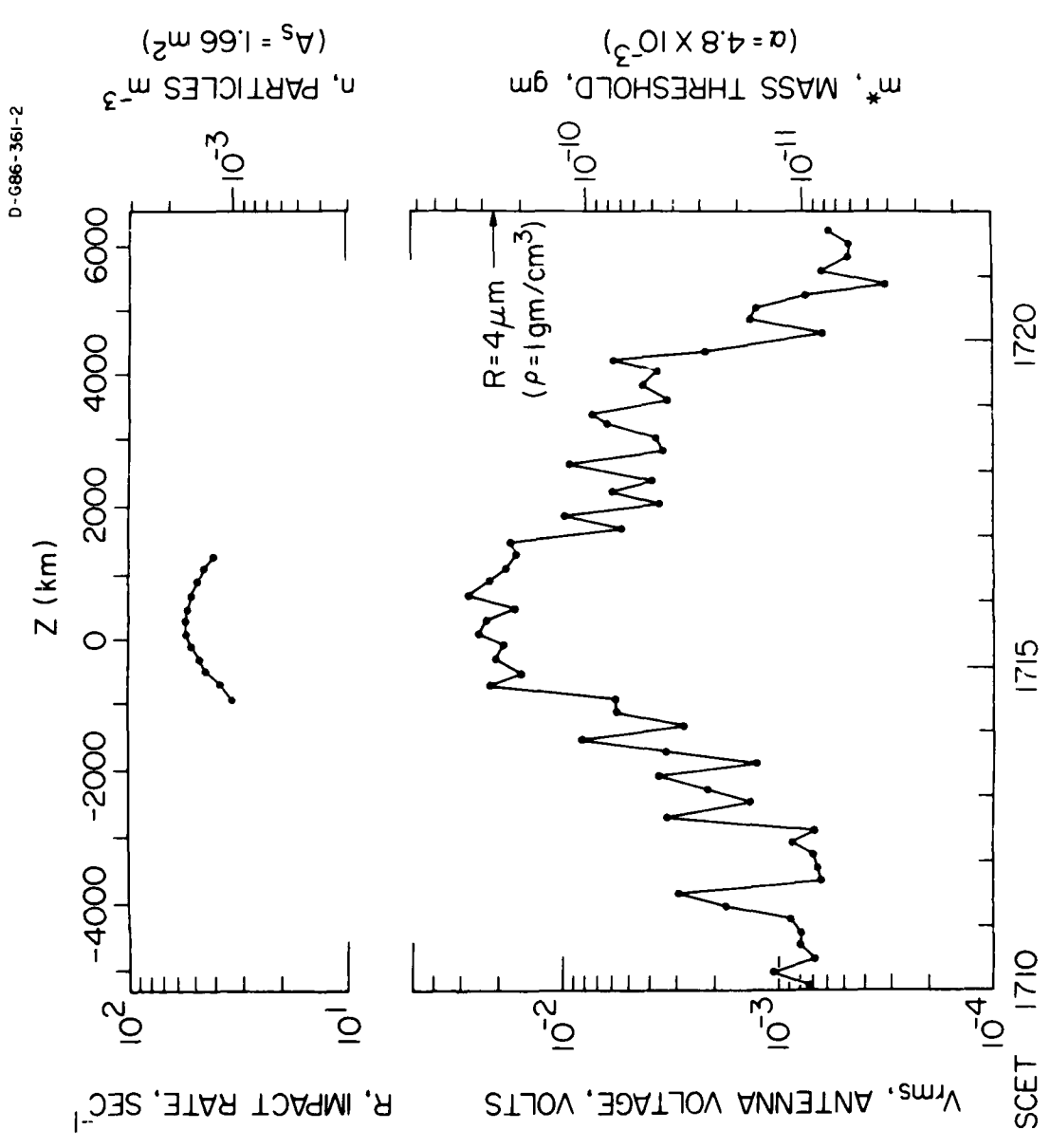
D-G86-361-2
n, PARTICLES m⁻³
(A_S = 1.66 m²)
m*, MASS THRESHOLD, gm
(α = 4.8 X 10⁻³)
Z (km)
R=4μm
(ρ=1gm/cm³)
R, IMPACT RATE, SEC⁻¹
V_rms, ANTENNA VOLTAGE, VOLTS
SCET
VOYAGER 2, JAN. 24, 1986

Figure 9

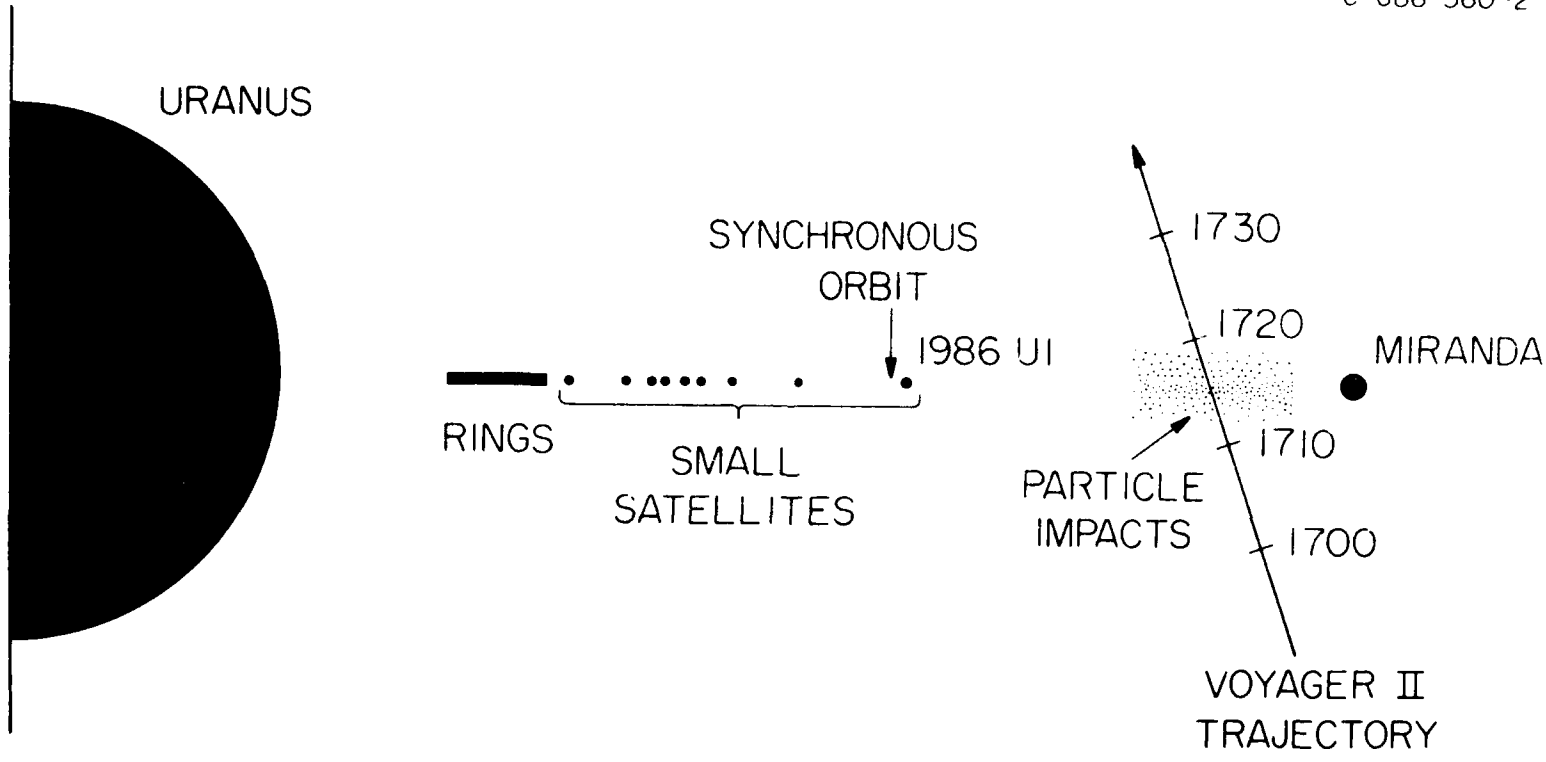
C-G86-360-2
URANUS
SYNCHRONOUS
ORBIT
1986 U1
RINGS
SMALL
SATELLITES
1730
1720
1710
1700
MIRANDA
PARTICLE
IMPACTS
VOYAGER II
TRAJECTORY

Figure 10